Contribution of low-lying vector resonances to polarization observables in $\bar{B}_d^0 \to \bar{K}^{*0} e^+ e^-$ decay

Alexander Yu. Korchin* and Vladimir A. Kovalchuk†

NSC Kharkov Institute of Physics and Technology, 61108 Kharkov, Ukraine

(Received 22 April 2010; revised manuscript received 1 July 2010; published 12 August 2010)

The branching ratio and other observables for the rare flavor-changing neutral current decay $\bar{B}_d^0 \to \bar{K}^{*0}(\to K^- \pi^+) e^+ e^-$ are studied below the $\bar{c}c$ threshold. The total amplitude for this decay includes the term coming from the standard model effective Hamiltonian and the term generated by the processes $\bar{B}_d^0 \to \bar{K}^{*0}(\to K^- \pi^+) V$ with intermediate low-lying vector resonances $V = \rho(770)$, $\omega(782)$, $\phi(1020)$ decaying into the $e^+ e^-$ pair. The resonance contribution to the branching ratio, polarization fractions of the K^* meson, and coefficients in the angular distribution is calculated. The influence of the resonances on the integrated observables in the region of electron-positron invariant mass up to 1 GeV is studied in view of the planned measurements of the photon polarization at the LHCb.

DOI: 10.1103/PhysRevD.82.034013 PACS numbers: 13.20.He, 12.40.Vv, 13.25.Hw

I. INTRODUCTION

The investigation of rare B decays induced by the flavor-changing neutral current (FCNC) transitions $b \to s$ and $b \to d$ represents an important test of the standard model (SM) and its extensions (see [1] for a review). Among the rare decays, the radiative decay $b \to s\gamma$ has probably been the most popular FCNC transition ever since its experimental observation as $B \to K^* \gamma$ at CLEO in 1993 [2]. This decay proceeds through a loop (penguin) diagram, to which high-mass particles introduced in extensions to the SM may contribute with a sizable amplitude. The size of the decay rate itself, however, provides only a mild constraint on such extensions, because the SM predictions for exclusive rates suffer from large and model-dependent form factor uncertainties [3,4]. Further reduction in the errors of the theory appears rather difficult. It is then clearly advantageous to use, in addition to the rates, other observables that can reveal new physics (NP).

In particular, in the framework of the SM, the photons emitted in $b \to s\gamma$ decays are predominantly left-handed, while those emitted in $\bar{b}$ decays are predominantly right-handed. Based on the leading order effective Hamiltonian, the amplitude for emission of wrong-helicity photons is suppressed by a factor $\propto m_s/m_b$ [5]. This suppression can easily be alleviated in a large number of NP scenarios where the helicity flip occurs on an internal line. An independent measurement of the photon helicity is therefore of interest. Several different methods of measuring the photon polarization have been suggested. In one method the photon helicity is probed through mixing-induced CP asymmetries [5]. Another method makes use of the photons from the $B \to \gamma K^*(\to K\pi)$ decay, which are converted into the electron-positron pair in the detector material [6,7]. There are also other techniques to probe photon polarization. These include approaches in which interference between different resonances [8] or different helicity states [9] of the hadronic recoil system provide sensitivity to the polarization. The photon polarization may also be studied in radiative decays of Λ_b baryons [10]. It appears, however, that experimentally the photon polarization is difficult to measure, and one instead has to use the process $b \to s\gamma^* \to s\ell^+\ell^-$, where the photon is converted to the lepton pair. In this decay the angular distributions and lepton polarizations can probe the chiral structure of the matrix element [6,11–16] and thereby the NP effects.

In order to unambiguously measure effects of NP in the process $b \to s\ell^+\ell^-$, if they indeed show up in the observables, one needs to calculate the SM predictions with a rather good accuracy. In general, the SM amplitude consists of the short-distance (SD) contributions and the long-distance (LD) ones. The former are expressed in terms of the Wilson coefficients C_i calculated in perturbative QCD up to a certain order in $\alpha_s(\mu)$; they carry information on processes at energy scales $\sim m_W$, m_t [here $\alpha_s(\mu)$ is the effective QCD coupling constant]. These coefficients are then evolved, using the renormalization group methods, to the energies related to the bottom quark mass m_b.

The LD terms include factorizable and nonfactorizable effects from virtual photons via the semileptonic operators $\mathcal{O}_{9V,10A}$ and electromagnetic dipole penguin operator $\mathcal{O}_{7\gamma}$ in the effective Hamiltonian. The radiative corrections coming from the operators $\mathcal{O}_{1-6}$ and the gluon penguin operator $\mathcal{O}_{8g}$ are also accurately accounted for (for a review, see [17]).

The LD effects describing the hadronization process are expressed in terms of hadronic matrix elements of the $b \to s$ operators between the initial B and the K^* final state. These matrix elements are parametrized in terms of form

*korchin@kipt.kharkov.ua
†koval@kipt.kharkov.ua

factors [12] that are calculated with the help of light-cone sum rules (LCSR) [18] or in soft-collinear effective theory [19]. The form factors have large theoretical uncertainties that are presently the dominant uncertainties in the SM predictions for exclusive decays.

The presence of additional LD effects originating from intermediate vector resonances $\rho(770)$, $\omega(782)$, $\phi(1020)$, $J/\psi(1S)$, $\psi(2S)$, ... complicates the description and makes it more model dependent. These resonances show up in the region of relatively small dilepton invariant mass $m_{ee} \equiv \sqrt{q^2}$, where $q^2 = (q_+ + q_-)^2$. In order to suppress the charmonia contribution, often the region of large dilepton mass ($q^2 \gg 4m_c^2 \approx 6.5\ \mathrm{GeV}^2$) is selected; for example, *BABAR* and Belle Collaborations apply the corresponding experimental cuts [20,21]. In some cases the resonances $J/\psi(1S)$, $\psi(2S)$ are explicitly excluded in the analysis via the Breit-Wigner energy factors.

The region of small dilepton invariant mass, $m_{ee} \lesssim 1$ GeV, has attracted less attention so far. Nevertheless, as was pointed out in [6], this region also has a high potential for searching for NP effects. At small $m_{ee} \sim M_R$ the low-lying vector resonances modify the amplitude and thus may induce, in certain observables, the right-handed photon polarization, which is still small but not negligible. The presence of the photon propagator $1/q^2$ enhances the resonance contribution. Recently, the authors of [22] analyzed the angular distribution in the rare decay $\bar{B}^0 \to \bar{K}^{*0} e^+ e^-$ in the small-q^2 region, in order to test the possibility to measure this distribution at the LHCb. They have shown the feasibility of future measurements with small systematic uncertainties.

In the present paper we calculate the branching fraction $d\Gamma/dq^2$ and asymmetries in the $\bar{B}^0 \to \bar{K}^{*0} e^+ e^-$ decay at dilepton invariant mass $m_{ee} < 2.5$ GeV. Both the SD and LD effects in the amplitude are evaluated. We use the effective Hamiltonian with the Wilson coefficients in the next-to-next-to-leading order (NNLO) approximation. The LD effects mediated by the resonances, i.e. $\bar{B}^0 \to \bar{K}^{*0} V \to \bar{K}^{*0} \gamma^* \to \bar{K}^{*0} e^+ e^-$ with $V = \rho(770)$, $\omega(782)$, $\phi(1020)$, are included explicitly in terms of amplitudes of the decays $\bar{B}^0 \to \bar{K}^{*0} V$. The information on the latter amplitudes is taken from experiment if available; otherwise it is taken from theoretical predictions.

We also study the sensitivity of the observables in the $\bar{B}^0 \to \bar{K}^{*0} e^+ e^-$ decay to the choice of the form factors of the transition $B \to K^*$. In the literature there exists a large variety of models for these form factors. We choose a few models [12,18,23,24] in our calculation. The other nontrivial aspect of the theory is the mass of the strange quark m_s, as a nonzero value of m_s leads to a small admixture of the right-handed photon polarization. Therefore, we calculate observables with both zero and nonzero values of the strange quark mass.

We calculate the coefficients $A_{\mathrm{T}}^{(2)}$ and A_{Im}, which determine, respectively, $\cos(2\phi)$ and $\sin(2\phi)$ dependencies in the angular distributions of the leptons (ϕ is the angle between the plane spanned by e^+, e^- and the plane spanned by the decay products K^-, π^+ of the $\bar{K}^{*0}$ meson). The other observables, such as forward-backward asymmetry dA_{FB}/dq^2 and polarization parameters of K^* meson f_0, $f_\parallel$, $f_\perp$, are also calculated.

The paper is organized as follows. In Sec. II the main formulas for the calculation of observables are presented. In Sec. II A the expressions for the fully differential decay rate and partially integrated ones over the angles and the dilepton invariant mass are given. Section II B contains expressions for transversity amplitudes in the SM, and the amplitudes in the limit of very small q^2. Contributions of the resonances $\rho(770)$, $\omega(782)$, $\phi(1020)$, and all ingredients needed for their calculation, are discussed in Sec. II C. Results of the calculations and a discussion are presented in Sec. III. In Sec. IV we draw our conclusions. In Appendix A some details of the calculation of the matrix element and the models of the $B \to K^*$ transition form factors are described.

II. ANGULAR DISTRIBUTIONS AND AMPLITUDES FOR THE $\bar{B}_d^0 \to \bar{K}^{*0} e^+ e^-$ DECAY

A. Differential decay rate

The decay $\bar{B}_d^0 \to \bar{K}^{*0} e^+ e^-$, with $\bar{K}^{*0} \to K^- \pi^+$ on the mass shell [25], is completely described by four independent kinematic variables: the electron-positron pair invariant mass squared, q^2, and the three angles θ_1, θ_2, ϕ. In the helicity frame (Fig. 1), the angle $\theta_1(\theta_2)$ is defined as the angle between the directions of motion of $e^+(K^-)$ in the $\gamma^*(\bar{K}^{*0})$ rest frame and the $\gamma^*(\bar{K}^{*0})$ in the $\bar{B}_d^0$ rest frame. The azimuthal angle ϕ is defined as the angle between the decay planes of $\gamma^* \to e^+ e^-$ and $\bar{K}^{*0} \to K^- \pi^+$ in the $\bar{B}_d^0$ rest frame. The differential decay rate in these coordinates is given by

$$\frac{d^4\Gamma}{d\hat{q}^2 d\cos\theta_1 d\cos\theta_2 d\phi} = m_B \frac{9}{64\pi} \sum_{k=1}^{9} a_k(q^2) g_k(\theta_1, \theta_2, \phi), \tag{1}$$

where the angular terms g_k are defined as

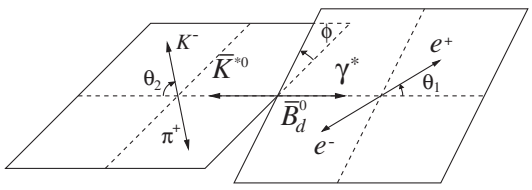

FIG. 1. Definition of helicity angles θ_1, θ_2, and ϕ, for the decay $\bar{B}_d^0 \to \bar{K}^{*0} e^+ e^-$.

$$g_1 = 4\sin^2\theta_1\cos^2\theta_2, \qquad g_2 = (1+\cos^2\theta_1 - \sin^2\theta_1\cos2\phi)\sin^2\theta_2, \qquad g_3 = (1+\cos^2\theta_1 + \sin^2\theta_1\cos2\phi)\sin^2\theta_2,$$
$$g_4 = -2\sin^2\theta_1\sin^2\theta_2\sin2\phi, \qquad g_5 = -\sqrt{2}\sin2\theta_1\sin2\theta_2\cos\phi, \qquad g_6 = -\sqrt{2}\sin2\theta_1\sin2\theta_2\sin\phi,$$
$$g_7 = 4\cos\theta_1\sin^2\theta_2, \qquad g_8 = -2\sqrt{2}\sin\theta_1\sin2\theta_2\cos\phi, \qquad g_9 = -2\sqrt{2}\sin\theta_1\sin2\theta_2\sin\phi,$$

and the amplitude terms a_k as

$$a_1 = |A_0|^2, \qquad a_2 = |A_\parallel|^2, \qquad a_3 = |A_\perp|^2, \qquad a_4 = \mathrm{Im}(A_\parallel A_\perp^*), \qquad a_5 = \mathrm{Re}(A_0 A_\parallel^*), \qquad a_6 = \mathrm{Im}(A_0 A_\perp^*),$$
$$a_7 = \mathrm{Re}(A_{\parallel L}A_{\perp L}^* - A_{\parallel R}A_{\perp R}^*), \qquad a_8 = \mathrm{Re}(A_{0L}A_{\perp L}^* - A_{0R}A_{\perp R}^*), \qquad a_9 = \mathrm{Im}(A_{0L}A_{\parallel L}^* - A_{0R}A_{\parallel R}^*),$$

where m_B is the mass of the B_d^0 meson, $\hat{q}^2 \equiv q^2/m_B^2$, and

$$A_i A_j^* \equiv A_{iL}(q^2)A_{jL}^*(q^2) + A_{iR}(q^2)A_{jR}^*(q^2).$$

Here $i, j = (0, \parallel, \perp)$, the electron mass m_e is neglected, and $A_{0L(R)}$, $A_{\parallel L(R)}$, and $A_{\perp L(R)}$ are the complex decay amplitudes of the three helicity states in the transversity basis.

With its rich multidimensional structure, the differential decay rate in Eq. (1) has sensitivity to various effects modifying the SM, such as *CP* violation beyond the Cabibbo-Kobayashi-Maskawa mechanism and/or right-handed currents. Given sufficient data, all a_k can, in principle, be completely measured from the full angular distribution in all three angles θ_1, θ_2, and ϕ.

The familiar electron-positron pair invariant-mass spectrum for $\bar{B}_d^0 \to \bar{K}^{*0}e^+e^-$ decay can be recovered after integration over all angles as

$$\frac{d\Gamma}{d\hat{q}^2} = m_B(|A_0|^2 + |A_\parallel|^2 + |A_\perp|^2). \tag{2}$$

The longitudinal and transverse partial widths are given, respectively, by

$$\frac{d\Gamma_0}{d\hat{q}^2} = m_B|A_0|^2, \qquad \frac{d\Gamma_\mathrm{T}}{d\hat{q}^2} \equiv \frac{d\Gamma_\parallel}{d\hat{q}^2} + \frac{d\Gamma_\perp}{d\hat{q}^2}.$$

The fraction of K^* meson polarization is $[i = (0, \parallel, \perp)]$

$$f_i = \frac{d\Gamma_i}{d\hat{q}^2}\Big/\frac{d\Gamma}{d\hat{q}^2}, \qquad \frac{d\Gamma_i}{d\hat{q}^2} = m_B|A_i|^2,$$

and $f_\mathrm{T} = f_\parallel + f_\perp = 1 - f_0$. Integrating Eq. (1) over the variables $\cos\theta_1$ and ϕ, we obtain

$$\frac{d^2\Gamma}{d\hat{q}^2 d\cos\theta_2} = \frac{3}{4}\frac{d\Gamma_\mathrm{T}}{d\hat{q}^2}(1 + \alpha_{K^*}\cos^2\theta_2), \tag{3}$$

where α_{K^*} is the K^* meson polarization parameter, $\alpha_{K^*} \equiv 2f_0/f_\mathrm{T} - 1$. Integration of Eq. (1) over $\cos\theta_2$ and ϕ yields

$$\frac{d^2\Gamma}{d\hat{q}^2 d\cos\theta_1} = \frac{3}{4}\frac{d\Gamma_0}{d\hat{q}^2}\sin^2\theta_1 + \frac{3}{8}\frac{d\Gamma_\mathrm{T}}{d\hat{q}^2}(1+\cos^2\theta_1) + \frac{dA_\mathrm{FB}}{d\hat{q}^2}\cos\theta_1, \tag{4}$$

where A_FB is forward-backward asymmetry,

$$\frac{dA_\mathrm{FB}}{d\hat{q}^2} \equiv \int_{-1}^{1}\mathrm{sgn}(\cos\theta_1)\frac{d^2\Gamma}{d\hat{q}^2 d\cos\theta_1}d\cos\theta_1 = \frac{3m_B}{2}\mathrm{Re}(A_{\parallel L}A_{\perp L}^* - A_{\parallel R}A_{\perp R}^*),$$

and the normalized forward-backward asymmetries $d\bar{A}_\mathrm{FB}/d\hat{q}^2$ and $d\tilde{A}_\mathrm{FB}/d\hat{q}^2$ are given as

$$\frac{d\bar{A}_\mathrm{FB}}{d\hat{q}^2} \equiv \frac{dA_\mathrm{FB}}{d\hat{q}^2}\Big/\frac{d\Gamma}{d\hat{q}^2}, \qquad \frac{d\tilde{A}_\mathrm{FB}}{d\hat{q}^2} \equiv \frac{dA_\mathrm{FB}}{d\hat{q}^2}\Big/\frac{d\Gamma_\mathrm{T}}{d\hat{q}^2}. \tag{5}$$

Finally, the two-dimensional differential decay rate in q^2 and the angle ϕ between the lepton and meson planes, after integration over other variables, takes the form

$$\frac{d^2\Gamma}{d\hat{q}^2 d\phi} = \frac{1}{2\pi}\frac{d\Gamma}{d\hat{q}^2}\left(1 + \frac{1}{2}f_\mathrm{T}A_\mathrm{T}^{(2)}\cos2\phi - A_\mathrm{Im}\sin2\phi\right), \tag{6}$$

$$A_\mathrm{T}^{(2)} \equiv \frac{f_\perp - f_\parallel}{f_\mathrm{T}}, \qquad A_\mathrm{Im} \equiv m_B\mathrm{Im}(A_\parallel A_\perp^*)\Big/\frac{d\Gamma}{d\hat{q}^2}, \tag{7}$$

$$\tilde{A}_\mathrm{Im} \equiv m_B\mathrm{Im}(A_\parallel A_\perp^*)\Big/\frac{d\Gamma_\mathrm{T}}{d\hat{q}^2}. \tag{8}$$

For q^2-integrated quantities we introduce the notation

$$\langle X\rangle \equiv \int_{\hat{q}^2_\mathrm{min}}^{\hat{q}^2_\mathrm{max}}\frac{dX}{d\hat{q}^2}d\hat{q}^2,$$

where the X's are Γ or Γ_i. Integrated quantities $\langle f_i\rangle$, $\langle A_\mathrm{T}^{(2)}\rangle$, and $\langle A_\mathrm{Im}\rangle$, which are obtained from the ones above by integrating the numerator and the denominator separately over q^2, are defined as follows:

$$\langle f_i\rangle \equiv \frac{\langle\Gamma_i\rangle}{\langle\Gamma\rangle}, \quad (i = 0, \perp, \parallel), \qquad \langle A_\mathrm{T}^{(2)}\rangle \equiv \frac{\langle\Gamma_\perp\rangle - \langle\Gamma_\parallel\rangle}{\langle\Gamma_\perp\rangle + \langle\Gamma_\parallel\rangle},$$
$$\frac{d\langle\Gamma\rangle}{d\phi} = \frac{\langle\Gamma\rangle}{2\pi}\left(1 + \frac{1}{2}\langle f_\mathrm{T}\rangle\langle A_\mathrm{T}^{(2)}\rangle\cos2\phi - \langle A_\mathrm{Im}\rangle\sin2\phi\right),$$
$$\langle A_\mathrm{Im}\rangle \equiv m_B\frac{\langle\mathrm{Im}A_\parallel A_\perp^*\rangle}{\langle\Gamma\rangle},$$
$$\langle\mathrm{Im}A_\parallel A_\perp^*\rangle \equiv \int_{\hat{q}^2_\mathrm{min}}^{\hat{q}^2_\mathrm{max}}\mathrm{Im}(A_\parallel A_\perp^*)d\hat{q}^2.$$

B. Transversity amplitudes

The nonresonant amplitudes follow from the matrix element of the $\bar{B}_d^0(p) \to \bar{K}^{*0}(k,\epsilon)e^+(q_+)e^-(q_-)$ process in Eq. (A1),

$$A_{0L,R}^{\rm NR} = -\frac{N\hat{\lambda}^{1/4}}{2\hat{m}_{K^*}}\Big((C_{9V}^{\rm eff} \mp C_{10A})\Big((1-\hat{q}^2-\hat{m}_{K^*}^2) \times (1+\hat{m}_{K^*})A_1(q^2) - \hat{\lambda}\frac{A_2(q^2)}{1+\hat{m}_{K^*}}\Big) + 2(\hat{m}_b-\hat{m}_s)C_{7\gamma}^{\rm eff}\Big((1-\hat{q}^2+3\hat{m}_{K^*}^2)T_2(q^2) - \frac{\hat{\lambda}}{1-\hat{m}_{K^*}^2}T_3(q^2)\Big)\Big), \quad (9)$$

$$A_{\|L,R}^{\rm NR} = N(1-\hat{m}_{K^*}^2)\sqrt{2\hat{q}^2}\hat{\lambda}^{1/4}\Big((C_{9V}^{\rm eff} \mp C_{10A})\frac{A_1(q^2)}{1-\hat{m}_{K^*}} + 2\frac{\hat{m}_b-\hat{m}_s}{\hat{q}^2}C_{7\gamma}^{\rm eff}T_2(q^2)\Big), \quad (10)$$

$$A_{\perp L,R}^{\rm NR} = -N\sqrt{2\hat{q}^2}\hat{\lambda}^{3/4}\Big((C_{9V}^{\rm eff} \mp C_{10A})\frac{V(q^2)}{1+\hat{m}_{K^*}} + 2\frac{\hat{m}_b+\hat{m}_s}{\hat{q}^2}C_{7\gamma}^{\rm eff}T_1(q^2)\Big). \quad (11)$$

In the above formulas the definitions $\hat{m}_{K^*} \equiv m_{K^*}/m_B$, $\hat{\lambda} \equiv \lambda(1,\hat{q}^2,\hat{m}_{K^*}^2) = (1-\hat{q}^2)^2 - 2(1+\hat{q}^2)\hat{m}_{K^*}^2 + \hat{m}_{K^*}^4$, $\hat{m}_b \equiv \bar{m}_b(\mu)/m_B$, $\hat{m}_s \equiv \bar{m}_s(\mu)/m_B$ are used, where m_{K^*} is the mass of the K^{*0} meson, and

$$N = |V_{tb}V_{ts}^*|\frac{G_F m_B^2 \alpha_{\rm em}}{32\pi^2\sqrt{3\pi}}.$$

The transversity amplitudes in Eqs. (9)–(11) take a particularly simple form in the heavy-quark and large-energy limit. In fact, exploiting the form factor relations in Eqs. (A10)–(A16), we obtain

$$A_{0L,R}^{\rm NR} = -N\hat{\lambda}^{1/4}\Big((C_{9V}^{\rm eff} \mp C_{10A})\Big(\hat{m}_{K^*}(1+\hat{q}^2-\hat{m}_{K^*}^2)\xi_\perp(q^2) + \frac{\hat{\lambda}}{2\hat{m}_{K^*}}\xi_\|(q^2)\Big) + 2(\hat{m}_b-\hat{m}_s)C_{7\gamma}^{\rm eff}\Big(2\hat{m}_{K^*}\xi_\perp(q^2) + \frac{\hat{\lambda}}{2\hat{m}_{K^*}}\xi_\|(q^2)\Big)\Big), \quad (12)$$

$$A_{\|L,R}^{\rm NR} = N\sqrt{2\hat{q}^2}\hat{\lambda}^{1/4}\Big((C_{9V}^{\rm eff} \mp C_{10A})(1-\hat{q}^2+\hat{m}_{K^*}^2) + 2\frac{\hat{m}_b-\hat{m}_s}{\hat{q}^2}(1-\hat{q}^2-\hat{m}_{K^*}^2)C_{7\gamma}^{\rm eff}\Big)\xi_\perp(q^2), \quad (13)$$

$$A_{\perp L,R}^{\rm NR} = -N\sqrt{2\hat{q}^2}\hat{\lambda}^{3/4}\Big(C_{9V}^{\rm eff} \mp C_{10A} + 2\frac{\hat{m}_b+\hat{m}_s}{\hat{q}^2}C_{7\gamma}^{\rm eff}\Big)\xi_\perp(q^2). \quad (14)$$

From inspection of these formulas we infer the following features. The amplitudes (13) and (14) are expressed through the one form factor $\xi_\perp(q^2)$. The observables $A_{\rm T}^{(2)}$, $\tilde{A}_{\rm Im}$, and $d\tilde{A}_{\rm FB}/d\hat{q}^2$ do not depend on the functional form of the form factor $\xi_\perp(q^2)$, and therefore they can be used to study the Wilson coefficients.

In the region $q^2 \lesssim m_{K^*}^2 = 0.803\ {\rm GeV}^2$, the transversity amplitudes (12)–(14) take the form

$$A_{0L,R}^{\rm NR} \approx -\frac{N}{2\hat{m}_{K^*}}\Big((C_{9V}^{\rm eff} \mp C_{10A})\Big(2\hat{m}_{K^*}^2\xi_\perp(q^2) + \Big(1-\frac{5}{2}(\hat{q}^2+\hat{m}_{K^*}^2)\Big)\xi_\|(q^2)\Big) + 2(\hat{m}_b-\hat{m}_s)C_{7\gamma}^{\rm eff}\Big(4\hat{m}_{K^*}^2\xi_\perp(q^2) + \Big(1-\frac{5}{2}(\hat{q}^2+\hat{m}_{K^*}^2)\Big)\xi_\|(q^2)\Big)\Big), \quad (15)$$

$$A_{\|L,R}^{\rm NR} \approx N\sqrt{\frac{2}{\hat{q}^2}}\Big((C_{9V}^{\rm eff} \mp C_{10A})\hat{q}^2 + 2(\hat{m}_b-\hat{m}_s) \times \Big(1-\frac{3}{2}(\hat{q}^2+\hat{m}_{K^*}^2)\Big)C_{7\gamma}^{\rm eff}\Big)\xi_\perp(q^2), \quad (16)$$

$$A_{\perp L,R}^{\rm NR} \approx -N\sqrt{\frac{2}{\hat{q}^2}}\Big((C_{9V}^{\rm eff} \mp C_{10A})\hat{q}^2 + 2(\hat{m}_b+\hat{m}_s) \times \Big(1-\frac{3}{2}(\hat{q}^2+\hat{m}_{K^*}^2)\Big)C_{7\gamma}^{\rm eff}\Big)\xi_\perp(q^2). \quad (17)$$

It follows from these equations that, in the region of very small invariant masses, namely, $q^2 \ll m_{K^*}^2$, the asymmetry $A_{\rm T}^{(2)}$ in Eq. (7) takes the simple form

$$A_{\rm T}^{(2)} \approx \frac{2m_s}{m_b}. \quad (18)$$

This result is in agreement with the well-known fact that, in the SM for $m_s = 0$ in a naive factorization, $A_{\rm T}^{(2)} = 0$ [13].

In some extensions of the SM, such as the left-right model and the unconstrained supersymmetric SM, there are right-handed currents in the matrix element, with the magnitude determined by the coupling $C_{7\gamma}^{\prime\,\rm eff}$ (see, e.g., Ref. [13]). In this case the asymmetry $A_{\rm T}^{(2)}$ is written as

$$A_{\rm T}^{(2)} \approx \frac{2C_{7\gamma}^{\prime\,\rm eff}C_{7\gamma}^{\rm eff}}{(C_{7\gamma}^{\rm eff})^2 + (C_{7\gamma}^{\prime\,\rm eff})^2}. \quad (19)$$

C. Resonant contribution

Further, we add the LD contributions from the decays $\bar{B}^0_d \to \bar{K}^{*0}V$, where $V = \rho^0$, ω, ϕ mesons, followed by $V \to e^+e^-$ in the decay $\bar{B}^0_d \to \bar{K}^{*0}e^+e^-$ (see Fig. 2). Using the vector-meson dominance concept we obtain the amplitude including nonresonant and resonant parts,

$$A_{\lambda L,R} = A^{\rm NR}_{\lambda L,R} + \sum_V \frac{c_V e^{i\delta_V}}{D_V(\hat{q}^2)} \left(\frac{\lambda(1,\hat{q}^2,\hat{m}^2_{K^*})}{\lambda(1,\hat{m}^2_V,\hat{m}^2_{K^*})}\right)^{1/4} \frac{\hat{m}_V}{\sqrt{\hat{q}^2}} h^V_\lambda, \tag{20}$$

$$c_V = {\rm sgn}(Q_V)({\rm Br}(V \to e^+e^-) \times {\rm Br}(\bar{B}^0_d \to \bar{K}^{*0}V)\hat{m}_V\hat{\Gamma}_V/(2\pi m_B\tau_B))^{1/2}, \tag{21}$$

where $\lambda = (0, \|, \perp)$ and

$$D_V(\hat{q}^2) = \hat{q}^2 - \hat{m}^2_V + i\hat{m}_V\hat{\Gamma}_V(\hat{q}^2)$$

is the usual Breit-Wigner function for the V meson resonance shape with the energy-dependent width $\Gamma_V(q^2)$ [$\hat{\Gamma}_V(\hat{q}^2) = \Gamma_V(q^2)/m_B$]. In Eq. (21) Q_V is the effective electric charge of the quarks in the vector meson V ($Q_\rho = 1/\sqrt{2}$, $Q_\omega = 1/\sqrt{18}$, $Q_\phi = -1/3$), $\hat{m}_V \equiv m_V/m_B$, $\hat{\Gamma}_V \equiv \Gamma_V/m_B$, $m_V(\Gamma_V)$ is the mass (width) of a V meson, Br(…) is the branching ratio, and τ_B is the lifetime of a B meson. In addition, h^V_λ ($\lambda = 0, \|, \perp$) are the complex amplitudes for $\bar{B}^0_d \to \bar{K}^{*0}V$ decay processes of the three helicity states in the transversity basis with the normalization condition $|h^V_0|^2 + |h^V_\||^2 + |h^V_\perp|^2 = 1$, and δ_V is the phase of the resonant amplitude relative to the phase of the nonresonant one.

Parameters of the vector resonances are presented in Table I. The energy-dependent width for the ρ meson is chosen as [26]

$$\Gamma_\rho(q^2) = \Gamma_\rho \frac{m_\rho}{\sqrt{q^2}} \frac{k^3}{k^3_0} \frac{1 + r^2k^2_0}{1 + r^2k^2} \Theta(q^2 - 4m^2_\pi), \tag{22}$$

where $k = (q^2/4 - m^2_\pi)^{1/2}$, $k_0 = (m^2_\rho/4 - m^2_\pi)^{1/2}$ and the parameter $r = 2.5\ {\rm GeV}^{-1}$ [27], $\Theta(x) = 1$ for $x \geq 0$, and $\Theta(x) = 0$ otherwise.

For the ω meson we take the energy dependence of the width in the form

$$\Gamma_\omega(q^2) = \Gamma_\omega[{\rm Br}(\omega \to 3\pi)\Theta(q^2 - 9m^2_\pi) + {\rm Br}(\omega \to \pi^0\gamma)\Theta(q^2 - m^2_\pi) + {\rm Br}(\omega \to 2\pi)\Theta(q^2 - 4m^2_\pi)],$$

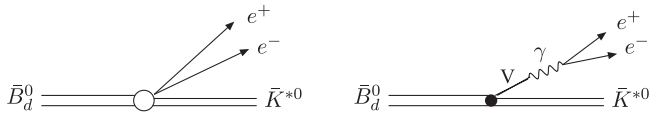

FIG. 2. Nonresonant and resonant contributions to the decay amplitude.

TABLE I. Mass, width, and leptonic branching ratio of the ρ^0, ω, and ϕ mesons [26].

V	m_V (GeV)	Γ_V (GeV)	Br($V \to e^+e^-$)
ρ^0	0.775 49	0.1462	4.71×10^{-5}
ω	0.782 65	0.008 49	7.16×10^{-5}
ϕ	1.019 455	0.004 26	2.97×10^{-4}

where the branching ratios are Br($\omega \to 3\pi$) = 89.2%, Br($\omega \to \pi^0\gamma$) = 8.92%, and Br($\omega \to 2\pi$) = 1.53% [26], and for the ϕ meson,

$$\Gamma_\phi(q^2) = \Gamma_\phi[{\rm Br}(\phi \to K^+K^-)\Theta(q^2 - 4m^2_{K^\pm}) + {\rm Br}(\phi \to K^0\bar{K}^0)\Theta(q^2 - 4m^2_{K^0}) + {\rm Br}(\phi \to 3\pi)\Theta(q^2 - 9m^2_\pi) + {\rm Br}(\phi \to \eta\gamma)\Theta(q^2 - m^2_\eta)],$$

with the branching ratios Br($\phi \to K^+K^-$) = 49.2%, Br($\phi \to K^0\bar{K}^0$) = 34.0%, Br($\phi \to 3\pi$) = 15.25%, and Br($\phi \to \eta\gamma$) = 1.304% [26].

In order to calculate the resonant contribution to the amplitude of the $\bar{B}^0_d \to \bar{K}^{*0}e^+e^-$ decay, one has to know the amplitudes of the decays $\bar{B}^0_d \to \bar{K}^{*0}\rho$, $\bar{B}^0_d \to \bar{K}^{*0}\omega$, and $\bar{B}^0_d \to \bar{K}^{*0}\phi$. Unfortunately, at present only the amplitude of the $\bar{B}^0_d \to \bar{K}^{*0}\phi$ decay is known from experiment [28]; therefore, in our estimate we use the amplitudes of the $\bar{B}^0_d \to \bar{K}^{*0}\rho$ and $\bar{B}^0_d \to \bar{K}^{*0}\omega$ decays from the theoretical prediction [29]. The absolute values and phase of the normalized decay amplitudes h^V_λ are shown in Table II.

III. RESULTS OF THE CALCULATION FOR THE $\bar{B}^0_d \to \bar{K}^{*0}e^+e^-$ DECAY AND A DISCUSSION

The parameters of the model are indicated in Table III. The SM Wilson coefficients at the scale $\mu = 4.8$ GeV to NNLO accuracy [15] are given in Table IV.

A. Invariant-mass distributions

In Figs. 3–6 we present results for the invariant-mass dependence of various observables for the $\bar{B}^0_d \to \bar{K}^{*0}e^+e^-$ decay. The upper limit of the invariant-mass region, 2.5 GeV, is taken to exclude the contribution from $J/\psi(1S)$ and higher resonances. Of course, the presented

TABLE II. Branching ratios [28] and decay amplitudes for $\bar{B}^0_d \to \bar{K}^{*0}\rho^0$ [29], $\bar{B}^0_d \to \bar{K}^{*0}\omega$ [29], and $\bar{B}^0_d \to \bar{K}^{*0}\phi$ [28].

Mode	$\bar{K}^{*0}\rho^0$	$\bar{K}^{*0}\omega$	$\bar{K}^{*0}\phi$
Br($\bar{B}^0_d \to \bar{K}^{*0}V$)	3.4×10^{-6}	2.0×10^{-6}	9.8×10^{-6}
$\lvert h^V_0\rvert^2$	0.70	0.75	0.480
$\lvert h^V_\perp\rvert^2$	0.14	0.12	0.241
arg($h^V_\|/h^V_0$) (rad)	1.17	1.79	2.40
arg($h^V_\perp/h^V_0$) (rad)	1.17	1.82	2.39

TABLE III. The numerical input used in our analysis.

$\lvert V_{tb}V_{ts}^*\rvert = 0.0407$	$G_F = 1.166\,37 \times 10^{-5}$ GeV^{-2}
$\mu = m_b = 4.8$ GeV	$\alpha_{\rm em} = 1/137$
$m_c = 1.4$ GeV	$m_B = 5.279\,53$ GeV
$\bar{m}_b(\mu) = 4.14$ GeV	$\tau_B = 1.530$ ps
$\bar{m}_s(\mu) = 0.079$ GeV	$m_{K^*} = 0.896$ GeV

results may depend on the relative phase δ_V in Eq. (20). In the figures below we choose this phase to be equal for all resonances ρ, ω, and ϕ, and equal to zero.

The polarization parameter f_0 for K^* is shown in Fig. 3 (recall that the transverse polarization fraction is related to f_0 through $f_T = 1 - f_0$). The resonances ρ, ω, and ϕ show up as small irregularities on the smooth curves. These parameters are calculated for the mass of the strange quark $m_s = 79$ MeV. The results of the calculation for $m_s = 0$ are not shown because they are indistinguishable from the curves for $m_s = 79$ MeV. One can also see a certain dependence on the choice of form factors.

The asymmetry $A_{\rm T}^{(2)}$ in the SM without and with resonant contributions is presented in Fig. 4. This observable turns out to be sensitive to all ingredients of the model. The dependence on the form factor model is quite essential, especially if resonances are not included (left-hand side).

TABLE IV. The SM Wilson coefficients at the scale $\mu = 4.8$ GeV, to NNLO accuracy. Input: $\alpha_s(m_W) = 0.120$, $\alpha_s(\mu) = 0.214$, obtained from $\alpha_s(m_Z) = 0.1176$ [26], using three-loop evolution, $\bar{m}_t(\bar{m}_t) = 162.3$ GeV, $m_W = 80.4$ GeV, and $\sin^2\theta_W = 0.23$.

$\bar{C}_1(\mu)$	$\bar{C}_2(\mu)$	$\bar{C}_3(\mu)$	$\bar{C}_4(\mu)$	$\bar{C}_5(\mu)$
-0.128	1.052	0.011	-0.032	0.009
$\bar{C}_6(\mu)$	$C_{7\gamma}^{\rm eff}(\mu)$	$C_{8g}^{\rm eff}(\mu)$	$C_{9V}(\mu)$	$C_{10A}(\mu)$
-0.037	-0.304	-0.167	4.211	-4.103

The addition of the resonances drastically changes this observable (see the right-hand side of Fig. 4). In particular, the ϕ meson contribution is very pronounced.

$A_{\rm T}^{(2)}$ is also sensitive to the mass of the strange quark (compare the top and bottom panels of Fig. 4). In particular, comparing the top and bottom panels (with resonances), one concludes that, at an invariant mass below 0.5 GeV (where $q^2 \ll m_{K^*}^2$), for $m_s = 0$ $A_{\rm T}^{(2)}$ vanishes, while for $m_s = 79$ MeV $A_{\rm T}^{(2)}$ is about 0.04. This value is in agreement with Eq. (18). Note that this asymmetry is, in general, an important observable to study effects of NP [13]. Indeed, comparison of $A_{\rm T}^{(2)}$ for $m_s = 0$ and $m_s \neq 0$ demonstrates the effect of the "wrong" helicity transition $b_L \to s_R + \gamma_R$. In the SM this effect appears to be small, being proportional to the ratio $2m_s/m_b$, while in some extensions of the SM it can reach bigger values depending on the coefficient $C_{7\gamma}^{\prime\,\rm eff}$ in Eq. (19) (see, e.g., the estimates in [13]). It also follows that the effect of the nonzero mass m_s is bigger than the uncertainty related to the chosen model for the transition form factors.

In general, theoretical uncertainties of the nonresonant amplitudes arise due to the choice of the renormalization scale μ (the scale at which the Wilson coefficients, α_s, and $\overline{\rm MS}$ masses are calculated), the ratio m_c/m_b, and some other uncertainties [30]. There are also corrections of the order $\Lambda_{\rm QCD}/m_b$ which are evaluated in Refs. [15,16]. While it is assumed in [15] that the main part of the $\Lambda_{\rm QCD}/m_b$ corrections is inside the QCD form factors, the authors of [16] explicitly include these corrections in the amplitudes $A_{\lambda L,R}^{\rm NR}$. For an estimate of the theoretical error of the calculation of the asymmetry $A_{\rm T}^{(2)}$, we can use the result of [16], in which the $\Lambda_{\rm QCD}/m_b$ corrections to each spin amplitude are estimated to be $\pm 10\%$. That leads to the total uncertainty $A_{\rm T}^{(2)}$ about ± 0.05, in the SM with $m_s = 0$ (see Fig. 14 in [16]). In view of this, the effect of the nonzero

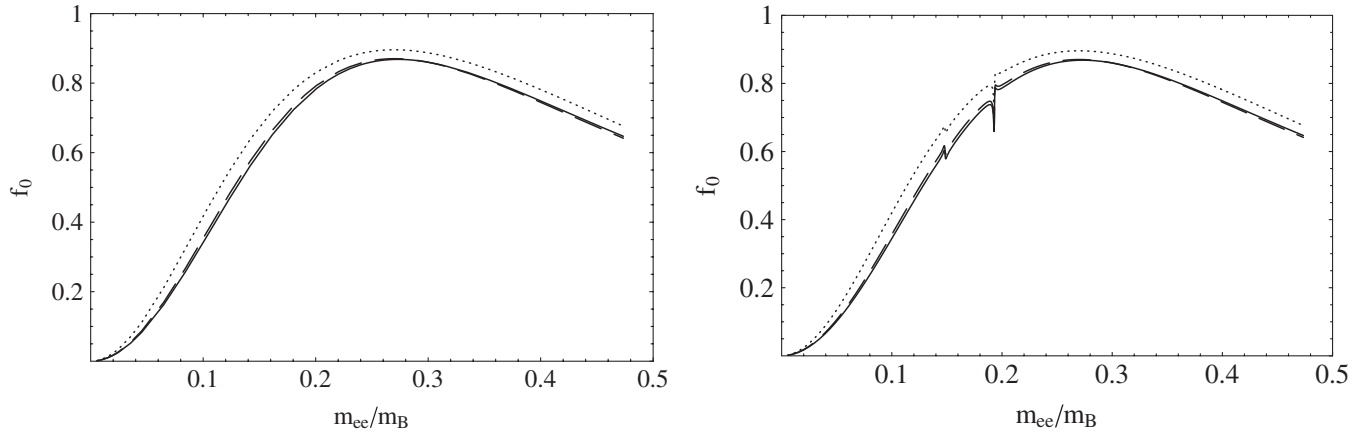

FIG. 3. Longitudinal polarization fraction of the K^* meson as a function of m_{ee}/m_B. Left (right) panel corresponds to the calculation without (with) resonances taken into account. The mass of the strange quark is $m_s = 79$ MeV. The dashed lines correspond to the form factor model from [18], the dotted lines correspond to the model from [12], and the solid lines are calculated according to Eqs. (A7)–(A9) and (A17).

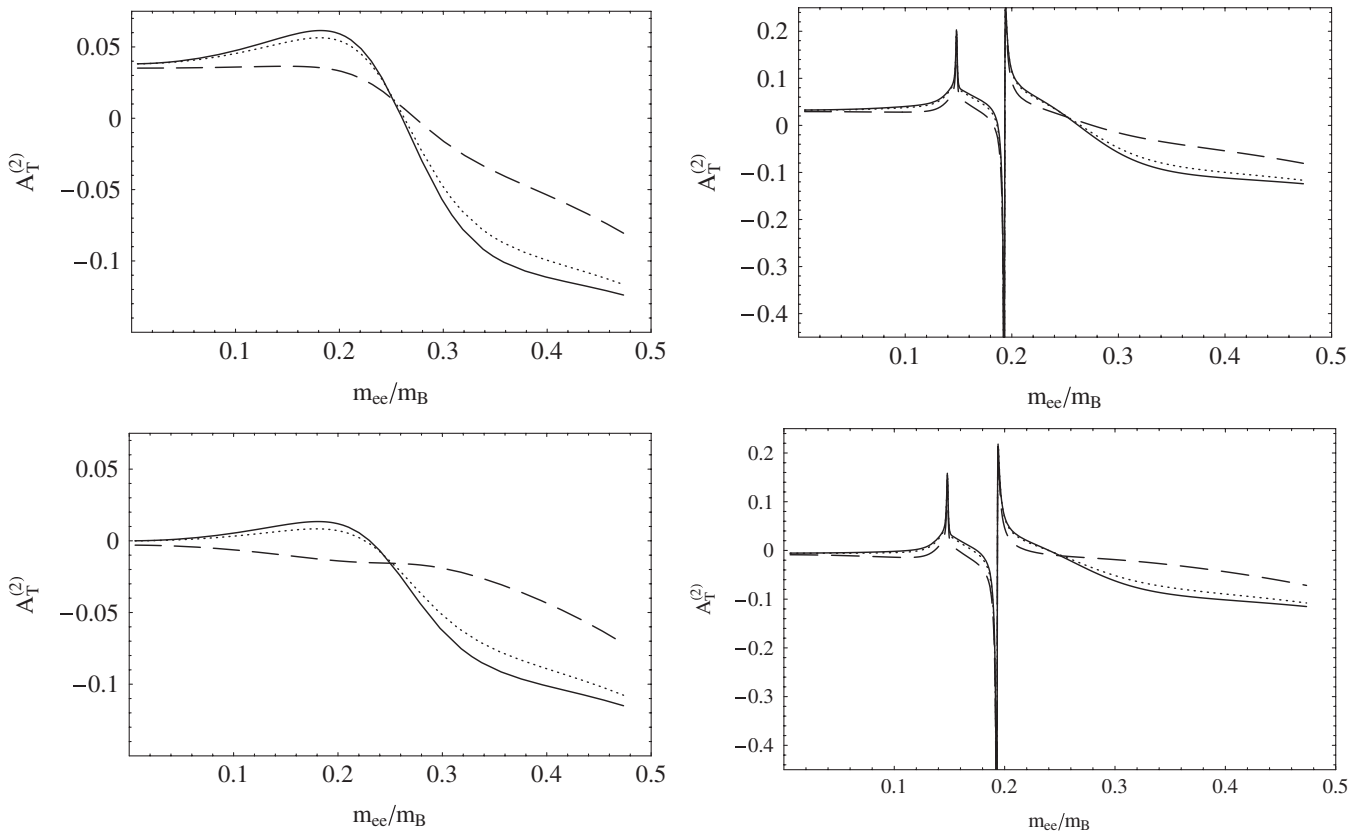

FIG. 4. Transverse asymmetry as a function of m_{ee}/m_B. Left (right) panels correspond to the calculation without (with) resonances taken into account. Top (bottom) panels correspond to the calculation with mass $m_s = 79$ MeV ($m_s = 0$). The lines are defined as in Fig. 3.

mass of the strange quark observed in Fig. 4 may be overshadowed by theoretical uncertainties, although this aspect requires further investigation.

Finally, in Figs. 5 and 6 we show the normalized forward-backward asymmetries in Eq. (5). Usually, for the normalized forward-backward asymmetry the quantity $d\bar{A}_{\rm FB}/d\hat{q}^2$ is chosen. Along with this one can define the forward-backward asymmetry $d\tilde{A}_{\rm FB}/d\hat{q}^2$, normalized in a different way [cf. Eq. (5)]. Comparing both figures we see that the latter asymmetry in Fig. 6 has interesting properties: (i) it is almost independent of the form factor model, and (ii) it may reach values up to ± 0.75 which are much larger than the maximal values taken by the asymmetry in Fig. 5. These properties, in our opinion, make $d\tilde{A}_{\rm FB}/d\hat{q}^2$ a

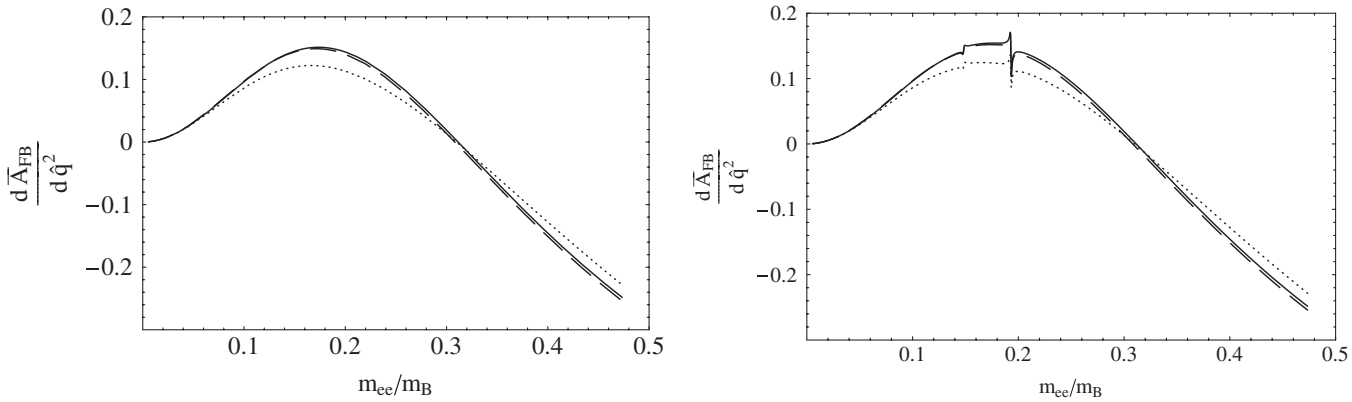

FIG. 5. The normalized forward-backward asymmetry $d\bar{A}_{\rm FB}/d\hat{q}^2$ as a function of m_{ee}/m_B. The left (right) panel corresponds to the calculation without (with) resonances taken into account. The mass of the strange quark is $m_s = 79$ MeV. The lines are defined as in Fig. 3.

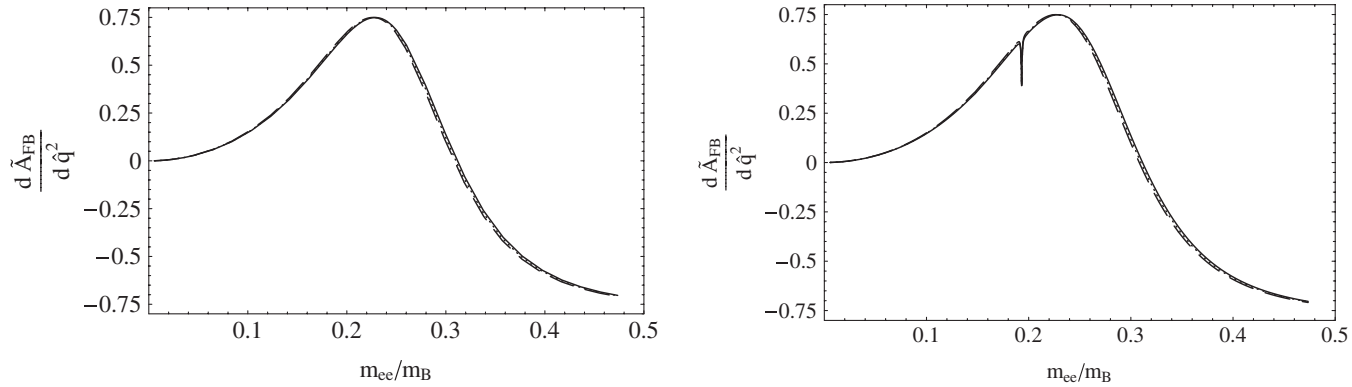

FIG. 6. The normalized forward-backward asymmetry $d\tilde{A}_{\rm FB}/d\hat{q}^2$ as a function of m_{ee}/m_B. The left (right) panel corresponds to the calculation without (with) resonances taken into account. The mass of the strange quark is $m_s = 79$ MeV. The lines are defined as in Fig. 3.

convenient observable for experimental study. Note that both these asymmetries change insignificantly when going from $m_s = 0$ to $m_s = 79$ MeV.

B. Observables integrated over q^2

In Tables V, VI, VII, and VIII we present results of the calculation of various observables in the framework of the SM, integrated over q^2. Two regions of e^+e^- invariant mass $m_{ee} \equiv \sqrt{q^2}$ are considered: (a) $0.030\,\text{GeV} < m_{ee} < 1\,\text{GeV}$ and (b) $0.5\,\text{GeV} < m_{ee} < 1\,\text{GeV}$. These intervals are selected because they turn out to be convenient for future experiments being planned at the LHCb (see Ref. [22]). In particular, the limit 0.030 GeV for interval (a) is taken because at lower masses, $m_{ee} <$ 0.030 GeV, it is difficult to define the plane of the lepton pair. When selecting interval (b) we took into account that the resolution on the ϕ angle in Fig. 1, according to the analysis of [22], for $m_{ee} > 0.5$ GeV is considerably better than the resolution for $m_{ee} < 0.5$ GeV. In addition, in region (b) the vector resonances ρ, ω, ϕ are expected to show up most prominently.

TABLE V. Predictions of the SM for the integrated branching ratio $\tau_B\langle\Gamma\rangle$, the polarization parameters $\langle f_i\rangle$, and the asymmetries $\langle A_{\rm T}^{(2)}\rangle$, $\langle A_{\rm Im}\rangle$ with the integration boundaries 0.030 GeV $\leq m_{ee} \leq$ 1 GeV. The contribution of the resonances ρ, ω, φ is not included. FF stands for the form factor model chosen according to [12,18] and Eqs. (A7)–(A9) and (A17).

	$m_s = 79$ MeV			$m_s = 0$		
	FF [12]	FF [18]	FF	FF [12]	FF [18]	FF
$\tau_B\langle\Gamma\rangle \times 10^7$	1.92	1.79	1.99	1.92	1.79	1.99
$\langle f_0\rangle$	0.25	0.20	0.19	0.25	0.20	0.19
$\langle f_\perp\rangle$	0.39	0.41	0.42	0.38	0.40	0.41
$\langle f_\parallel\rangle$	0.36	0.39	0.39	0.38	0.40	0.40
$\langle A_{\rm T}^{(2)}\rangle \times 10^2$	4.1	3.5	4.2	0.1	−0.4	0.2
$\langle A_{\rm Im}\rangle \times 10^5$	2.	1.	3.	1.	0.	2.

As seen from Tables V and VI, the branching ratio does not depend on the s quark mass, while it is sensitive to the form factors, especially in region (b).

The value of the K^* polarization fraction $\langle f_0\rangle$ does not change when varying the mass of the strange quark, while the polarization fractions $\langle f_\perp\rangle$, $\langle f_\parallel\rangle$ show weak dependence on value of m_s. Variations of all fractions with the form factor models are about 10%–20%. In region (a) the longitudinal polarization is smaller than the transverse ones, while in region (b) the longitudinal polarization prevails over the transverse ones.

As for the asymmetry $\langle A_{\rm T}^{(2)}\rangle$, one can notice its strong dependence on the choice of the form factors and especially on the value of the strange quark mass. Note that for the form factors, calculated using Eqs. (A7)–(A9) and (A17), this asymmetry is proportional to m_s if one neglects the mass of K^*. Then the $\langle A_{\rm T}^{(2)}\rangle$ value in the last column of these tables would be equal to zero. However, in our calculation we do not neglect the mass of K^*; therefore $\langle A_{\rm T}^{(2)}\rangle \neq 0$ for $m_s = 0$. For the nonzero value of m_s the calculated asymmetry is of the order 3%–5% depending on the choice of the form factors. The asymmetry $\langle A_{\rm Im}\rangle$ appears to be very small, on the level of 10^{-5}–10^{-4}.

Now we discuss the results with the total amplitude, including resonances (see Tables VII and VIII). In this

TABLE VI. Same as Table V but with the integration boundaries 0.5 GeV $\leq m_{ee} \leq$ 1 GeV.

	$m_s = 79$ MeV			$m_s = 0$		
	FF [12]	FF [18]	FF	FF [12]	FF [18]	FF
$\tau_B\langle\Gamma\rangle \times 10^8$	5.7	4.8	5.2	5.7	4.8	5.2
$\langle f_0\rangle$	0.62	0.56	0.55	0.62	0.56	0.55
$\langle f_\perp\rangle$	0.20	0.23	0.24	0.19	0.22	0.23
$\langle f_\parallel\rangle$	0.18	0.21	0.22	0.19	0.22	0.23
$\langle A_{\rm T}^{(2)}\rangle \times 10^2$	5.0	3.6	5.4	0.6	−0.9	0.9
$\langle A_{\rm Im}\rangle \times 10^5$	5.	2.	8.	3.	−1.	5.

calculation, for definiteness, the relative resonant phases δ_V for $V = \rho, \omega, \phi$ have been taken equal to each other. For the estimation, we have chosen three values of the phase: $-\pi/4$, 0, and $+\pi/4$.

Let us start with the branching ratio $\tau_B\langle\Gamma\rangle$. As seen by comparing Tables V and VI with Tables VII and VIII, in the q^2 interval (a) the resonant contribution is negligibly small. In interval (b) this contribution is bigger, at the level of 1%, which is still much smaller than the expectations of Ref. [22].

The polarization fractions of the K^* also do not change by more than ~5% after inclusion of the resonances, though $\langle f_i\rangle$ are more sensitive to the choice of the transition form factors $B \to K^*$.

On the contrary, the asymmetry $\langle A_{\rm T}^{(2)}\rangle$ receives a large contribution from the resonances. In the region $0.030\ \text{GeV} < m_{ee} < 1\ \text{GeV}$, this contribution can reach up to 15% depending on the choice of form factors and the resonant phase δ_V, while in the region $0.5\ \text{GeV} < m_{ee} < 1\ \text{GeV}$, the resonant contribution appears to be much smaller, ~3%. Of course, the asymmetry remains of the order of a few percent. We should emphasize the strong dependence of this observable on the choice of form factors.

This integrated asymmetry remains sensitive to the value of m_s, and therefore sensitive to the wrong helicity transition $b_L \to s_R + \gamma_R$. It also follows from our calculation that effects of NP should lead to values of $\langle A_{\rm T}^{(2)}\rangle \gtrsim 0.1$; otherwise, it will be difficult to distinguish these effects from all model uncertainties discussed above in Sec. III A.

TABLE VII. Predictions for the integrated branching ratio $\tau_B\langle\Gamma\rangle$, the polarization parameters $\langle f_i\rangle$, and the asymmetries $\langle A_{\rm T}^{(2)}\rangle$, $\langle A_{\rm Im}\rangle$ with the integration boundaries $0.030\ \text{GeV} \le m_{ee} \le 1\ \text{GeV}$. The long-distance contribution from ρ, ω, and φ mesons is added. FF stands for the form factor model chosen according to [12,18] and Eqs. (A7)–(A9) and (A17).

		$m_s = 79$ MeV			$m_s = 0$		
	δ_V	FF [12]	FF [18]	FF	FF [12]	FF [18]	FF
	$-\pi/4$	1.92	1.79	1.99	1.92	1.79	1.99
$\tau_B\langle\Gamma\rangle \times 10^7$	0	1.92	1.79	1.99	1.92	1.79	1.99
	$\pi/4$	1.92	1.79	1.99	1.91	1.79	1.99
	$-\pi/4$	0.25	0.20	0.19	0.25	0.20	0.19
$\langle f_0\rangle$	0	0.25	0.20	0.19	0.25	0.20	0.19
	$\pi/4$	0.24	0.20	0.19	0.24	0.20	0.19
	$-\pi/4$	0.39	0.41	0.42	0.38	0.40	0.40
$\langle f_\perp\rangle$	0	0.39	0.41	0.42	0.38	0.40	0.40
	$\pi/4$	0.39	0.42	0.42	0.38	0.40	0.41
	$-\pi/4$	0.36	0.39	0.39	0.38	0.40	0.41
$\langle f_\parallel\rangle$	0	0.36	0.39	0.39	0.38	0.40	0.41
	$\pi/4$	0.36	0.39	0.39	0.38	0.40	0.41
	$-\pi/4$	3.5	2.9	3.6	−0.5	−1.0	−0.4
$\langle A_{\rm T}^{(2)}\rangle \times 10^2$	0	3.6	3.0	3.7	−0.4	−1.0	−0.3
	$\pi/4$	3.9	3.4	4.0	0.	−0.6	0.1
	$-\pi/4$	0.6	0.6	0.6	0.6	0.6	0.6
$\langle A_{\rm Im}\rangle \times 10^3$	0	−1.2	−1.3	−1.2	−1.2	−1.3	−1.2
	$\pi/4$	−2.3	−2.4	−2.3	−2.3	−2.4	−2.3

TABLE VIII. Same as Table VII but with the integration boundaries $0.5\ \text{GeV} \le m_{ee} \le 1\ \text{GeV}$.

		$m_s = 79$ MeV			$m_s = 0$		
	δ_V	FF [12]	FF [18]	FF	FF [12]	FF [18]	FF
	$-\pi/4$	5.7	4.8	5.3	5.7	4.8	5.2
$\tau_B\langle\Gamma\rangle \times 10^8$	0	5.6	4.8	5.2	5.6	4.8	5.2
	$\pi/4$	5.6	4.7	5.2	5.6	4.7	5.2
	$-\pi/4$	0.62	0.56	0.55	0.62	0.56	0.55
$\langle f_0\rangle$	0	0.62	0.56	0.54	0.62	0.56	0.54
	$\pi/4$	0.62	0.56	0.54	0.62	0.56	0.54
	$-\pi/4$	0.20	0.23	0.24	0.19	0.22	0.23
$\langle f_\perp\rangle$	0	0.20	0.23	0.24	0.19	0.22	0.23
	$\pi/4$	0.20	0.23	0.24	0.19	0.22	0.23
	$-\pi/4$	0.18	0.21	0.21	0.19	0.22	0.23
$\langle f_\parallel\rangle$	0	0.18	0.21	0.22	0.19	0.22	0.23
	$\pi/4$	0.18	0.21	0.22	0.19	0.23	0.23
	$-\pi/4$	5.0	3.5	5.3	0.5	−1.0	0.8
$\langle A_{\rm T}^{(2)}\rangle \times 10^2$	0	5.0	3.6	5.3	0.5	−0.9	0.9
	$\pi/4$	5.0	3.6	5.4	0.6	−0.9	0.9
	$-\pi/4$	0.6	0.2	0.8	0.3	−0.1	0.5
$\langle A_{\rm Im}\rangle \times 10^4$	0	−0.2	−0.8	−0.1	−0.5	−1.1	−0.4
	$\pi/4$	−0.6	−1.1	−0.5	−0.8	−1.5	−0.8

As for the asymmetry $\langle A_{\rm Im}\rangle$, it changes drastically after adding the resonances (compare Tables V and VI with Tables VII and VIII), from values $\sim 10^{-5}$ without resonances to values $\sim 10^{-3}$ [in region (a)] and $\sim 10^{-4}$ [in region (b)] with resonances. Note that $\langle A_{\rm Im}\rangle$ is determined by the imaginary part of the amplitude. The latter in the SM (without resonances) is determined by the light-quark loop through the function $Y(q^2)$ [30], and therefore the imaginary part of the nonresonant amplitude appears to be very small, $\sim 10^{-5}$. It is not surprising that the imaginary part of the total amplitude in Eq. (20) is determined solely by the resonant contribution.

Of course, this observable strongly depends on the resonant phase δ_V; however, for any phase it remains small. Since this asymmetry is determined mainly by the resonant amplitude, it does not show prominent dependence on m_s, especially in region (a). For these reasons $\langle A_{\rm Im}\rangle$ is not very suitable for the study of the chiral structure of the decay amplitude. At the same time, the calculation shows that observation of this asymmetry at the level of ~1% or bigger will indicate effects beyond the SM.

IV. CONCLUSIONS

Branching ratios and other observables for the rare FCNC decay $\bar{B}_d^0 \to \bar{K}^{*0}(\to K^-\pi^+)e^+e^-$ have been studied in the region of electron-positron invariant mass

below the $\bar{c}c$ threshold. Our main emphasis has been placed on an accurate account of the mechanism $\bar{B}_d^0 \to \bar{K}^{*0}(\to K^-\pi^+)V$ with low-lying vector resonances $V = \rho(770)$, $\omega(782)$, $\phi(1020)$ decaying into the e^+e^- pair.

The invariant-mass dependence of the branching ratio and coefficients in the angular distribution of the lepton pair, $A_{\rm T}^{(2)}$, $A_{\rm Im}$, $d\bar{A}_{\rm FB}/dq^2$, has been calculated and studied. In view of the planned experiments at the LHCb, in which the observables integrated over the invariant mass will be measured [22], we also calculated the corresponding quantities.

In general, the resonant contribution appears to be small in the branching ratio, polarization parameters of the K^* meson, and forward-backward asymmetry. Nevertheless, some of the observables change drastically after adding the resonances to the pure SM contribution. In particular, the q^2 dependence of the asymmetry $A_{\rm T}^{(2)}$ gets considerably modified by the vector resonances. This observation is of importance in view of the sensitivity of $A_{\rm T}^{(2)}$ to the value of the strange quark mass, and thereby to the chiral-odd dipole transition $b_L \to s_R + \gamma_R$. Thus $A_{\rm T}^{(2)}$ is also sensitive to effects of NP which are related to the right-handed currents. Still, $A_{\rm T}^{(2)}$ in the SM with resonances is small, of the order of a few percent. The resonances also increase the asymmetry $A_{\rm Im}$ by at least 1 order of magnitude; however, this observable remains very small, 10^{-4}–10^{-3}, and therefore it is difficult to measure.

The calculated quantities depend on the model of transition form factors which have been considered. In general, the band due to different models is of the order of $\sim$5%. In this connection, we have introduced a new forward-backward asymmetry $d\tilde{A}_{\rm FB}/dq^2$, normalized differently compared to the standard definition. This modified forward-backward asymmetry has the advantages of being almost independent of the form factor model and of taking big values up to ± 0.75.

Most of the above features remain after integration of the observables over the e^+e^- invariant mass up to 1 GeV. Two integration regions have been selected which are particularly suitable for the planned future measurements at the LHCb [22]. The predictions for all integrated observables are given in the framework of the SM, taking into account low-lying vector resonances.

APPENDIX A: MATRIX ELEMENT AND FORM FACTORS

1. Matrix element

The effective Hamiltonian for the quark-level transition $b \to se^+e^-$ within the SM is well known and can be taken, e.g., from Ref. [1]. It is expressed in terms of the local operators $\mathcal{O}_i$ and Wilson coefficients C_i, where $i = 1, \ldots, 6, 7\gamma, 8g, 9V, 10A$.

The matrix element of this effective Hamiltonian for the nonresonant decay $\bar{B}_d^0(p) \to \bar{K}^{*0}(k,\epsilon)e^+(q_+)e^-(q_-)$ can be written, in the so-called naive factorization [1], as

$$\begin{aligned}\mathcal{M}_{\rm NR} = \frac{G_F\alpha_{\rm em}}{\sqrt{2}\pi} V_{ts}^* V_{tb}\Big(&\langle \bar{K}^{*0}(k,\epsilon)|\bar{s}\gamma_\mu P_L b|\bar{B}_d^0(p)\rangle \\ &\times (C_{9V}^{\rm eff}\bar{u}(q_-)\gamma^\mu v(q_+) + C_{10A}\bar{u}(q_-)\gamma^\mu\gamma_5 v(q_+)) \\ &- \frac{2}{q^2} C_{7\gamma}^{\rm eff}\langle \bar{K}^{*0}(k,\epsilon)|\bar{s}i\sigma_{\mu\nu}q^\nu(\bar{m}_b(\mu)P_R \\ &+ \bar{m}_s(\mu)P_L)b|\bar{B}_d^0(p)\rangle\bar{u}(q_-)\gamma^\mu v(q_+)\Big). \qquad \text{(A1)}\end{aligned}$$

Here, V_{ij} are the Cabibbo-Kobayashi-Maskawa matrix elements [31], G_F is the Fermi coupling constant, $\alpha_{\rm em}$ is the electromagnetic fine-structure constant, $P_{L,R} = (1 \mp \gamma_5)/2$ denote chiral projectors, and $\bar{m}_b(\mu)$ $[\bar{m}_s(\mu)]$ is the running bottom (strange) quark mass in the $\overline{\rm MS}$ scheme at the scale μ. Moreover, $\sigma_{\mu\nu} = \frac{i}{2}[\gamma_\mu, \gamma_\nu]$, $q_\mu = (q_+ + q_-)_\mu$, $C_{7\gamma}^{\rm eff} = C_{7\gamma} - (4\bar{C}_3 - \bar{C}_5)/9 - (4\bar{C}_4 - \bar{C}_6)/3$, $C_{9V}^{\rm eff} = C_{9V} + Y(q^2)$, where $Y(q^2)$ is given in Ref. [30].

The "barred" coefficients $\bar{C}_i$ (for $i = 1, \ldots, 6$) are defined as certain linear combinations of the C_i, such that the $\bar{C}_i$ coincide at leading logarithmic order with the Wilson coefficients in the standard basis [17]. The coefficients C_i are calculated at the scale $\mu = m_W$, in a perturbative expansion in powers of $\alpha_s(m_W)$, and are then evolved down to scales $\mu \sim m_b$ using the renormalization group equations.

The $\overline{\rm MS}$ mass $\bar{m}_b(\mu)$ can be related with the pole mass m_b at the scale $\mu = m_b$ through [32,33]

$$\bar{m}_b(m_b) = m_b\left(1 - \frac{4}{3}\frac{\alpha_s(m_b)}{\pi} - 10.167\left(\frac{\alpha_s(m_b)}{\pi}\right)^2 + \mathcal{O}\left(\left(\frac{\alpha_s(m_b)}{\pi}\right)^3\right)\right).$$

The expression for the next terms in this equation can be found in Ref. [33]. The mass of the strange quark can be determined from the spectral function sum rules or lattice QCD simulation [34]. The up-to-date value of m_s given by the PDG [26] is $\bar{m}_s(2\ {\rm GeV}) = 95 \pm 25$ MeV. Note that this running mass is evaluated at $\mu_0 = 2$ GeV with three active quark flavors. The evolution of the $\bar{m}_s(\mu)$ is governed by the renormalization group equation which has the solution [35]

$$\frac{\bar{m}_s(\mu)}{\bar{m}_s(\mu_0)} = \frac{f(\alpha_s(\mu)/\pi)}{f(\alpha_s(\mu_0)/\pi)},$$

with

$$f(x) = x^{4/9}(1 + 0.895\,062x + 1.371\,43x^2 + \mathcal{O}(x^3)).$$

2. Form factors of $B \to K^*$ transition

The hadronic part of the matrix element in Eq. (A1) describing the $B \to K^*e^+e^-$ transition can be parame-

trized in terms of $B \to K^*$ form factors, which usually are defined as

$$\langle \bar{K}^*(k,\epsilon)|\bar{s}\gamma_\mu b|\bar{B}(p)\rangle = \frac{2V(q^2)}{m_B + m_{K^*}}\varepsilon_{\mu\nu\alpha\beta}\epsilon^{\nu *}p^\alpha k^\beta, \tag{A2}$$

$$\begin{aligned}\langle \bar{K}^*(k,\epsilon)|\bar{s}\gamma_\mu\gamma_5 b|\bar{B}(p)\rangle &= i\epsilon^*_\mu(m_B + m_{K^*})A_1(q^2) \\ &\quad - i(\epsilon^*\cdot p)(p+k)_\mu \frac{A_2(q^2)}{m_B + m_{K^*}} \\ &\quad - i(\epsilon^*\cdot p)q_\mu \frac{2m_{K^*}}{q^2} \\ &\quad \times (A_3(q^2) - A_0(q^2)),\end{aligned} \tag{A3}$$

with

$$\begin{aligned}A_3(q^2) &= \frac{m_B + m_{K^*}}{2m_{K^*}}A_1(q^2) \\ &\quad - \frac{m_B - m_{K^*}}{2m_{K^*}}A_2(q^2), \\ A_0(0) &= A_3(0);\end{aligned}$$

$$\langle \bar{K}^*(k,\epsilon)|\bar{s}\sigma_{\mu\nu}q^\nu b|\bar{B}(p)\rangle = i2T_1(q^2)\varepsilon_{\mu\nu\alpha\beta}\epsilon^{\nu *}p^\alpha k^\beta, \tag{A4}$$

$$\begin{aligned}&\langle \bar{K}^*(k,\epsilon)|\bar{s}\sigma_{\mu\nu}\gamma_5 q^\nu b|\bar{B}(p)\rangle \\ &\quad = T_2(q^2)(\epsilon^*_\mu(P\cdot q) - (\epsilon^*\cdot q)P_\mu) \\ &\quad + T_3(q^2)(\epsilon^*\cdot q)\left(q_\mu - \frac{q^2}{P\cdot q}P_\mu\right),\end{aligned} \tag{A5}$$

with $T_1(0) = T_2(0)$. In the above equations, $q = p - k$, $P = p + k$, $p^2 = m_B^2$, $k^2 = m_{K^*}^2$, ϵ^μ is the polarization vector of the K^* meson, $\epsilon^* \cdot k = 0$, and $\varepsilon_{0123} = 1$.

In the numerical estimations, we use the form factors from LCSR calculations [12,18] as well as the large-energy-effective-theory form factors $\xi_\perp(q^2)$ and $\xi_\parallel(q^2)$ [23,24,30]. Form factors given in [12] are parametrized as follows

$$F(q^2) = F(0)\exp(c_1\hat{q}^2 + c_2\hat{q}^4), \tag{A6}$$

where $\hat{q}^2 \equiv q^2/m_B^2$. The coefficients in this parametrization are listed in Table IX. The q^2 dependence of the $B \to K^*$ form factors given in [18] is parametrized as

$$F(q^2) = \frac{r_1}{1 - q^2/m_R^2} + \frac{r_2}{1 - q^2/m_{\rm fit}^2}, \tag{A7}$$

TABLE IX. Input values for the parametrization (A6) of the $B \to K^*$ form factors.

	A_1	A_2	A_0	V	T_1	T_2	T_3
$F(0)$	0.294	0.246	0.412	0.399	0.334	0.334	0.234
c_1	0.656	1.237	1.543	1.537	1.575	0.562	1.230
c_2	0.456	0.822	0.954	1.123	1.140	0.481	1.089

$$F(q^2) = \frac{r_1}{1 - q^2/m_{\rm fit}^2} + \frac{r_2}{(1 - q^2/m_{\rm fit}^2)^2}, \tag{A8}$$

$$F(q^2) = \frac{r_2}{1 - q^2/m_{\rm fit}^2}, \tag{A9}$$

where the fit parameters $r_{1,2}$, m_R^2, and $m_{\rm fit}^2$ are shown in Table X. In the large-energy effective theory the seven *a priori* independent $B \to K^*$ form factors in Eqs. (A2)–(A5) can be expressed in terms of two universal form factors $\xi_\perp(q^2)$ and $\xi_\parallel(q^2)$ [23]:

$$A_1(q^2) = \frac{2E_{K^*}}{m_B + m_{K^*}}\xi_\perp(q^2), \tag{A10}$$

$$A_2(q^2) = \frac{m_B + m_{K^*}}{m_B}(\xi_\perp(q^2) - \xi_\parallel(q^2)), \tag{A11}$$

$$A_0(q^2) = \frac{E_{K^*}}{m_{K^*}}\xi_\parallel(q^2) + \frac{m_{K^*}}{m_B}(\xi_\perp(q^2) - \xi_\parallel(q^2)), \tag{A12}$$

$$V(q^2) = \frac{m_B + m_{K^*}}{m_B}\xi_\perp(q^2), \tag{A13}$$

$$T_1(q^2) = \xi_\perp(q^2), \tag{A14}$$

$$T_2(q^2) = \left(1 - \frac{q^2}{m_B^2 - m_{K^*}^2}\right)\xi_\perp(q^2), \tag{A15}$$

$$T_3(q^2) = \xi_\perp(q^2) - \left(1 - \frac{m_{K^*}^2}{m_B^2}\right)\xi_\parallel(q^2). \tag{A16}$$

Note the different convention for the longitudinal form factor with $\xi_\parallel(q^2) = m_{K^*}/E_{K^*}\zeta_\parallel(q^2)$, $\zeta_\parallel(q^2)$ being defined in Ref. [23]. Here, E_{K^*} is the energy of the final vector meson in the B rest frame,

$$E_{K^*} = \frac{m_B}{2}\left(1 - \frac{q^2}{m_B^2} + \frac{m_{K^*}^2}{m_B^2}\right).$$

The form factors $\xi_\perp(q^2)$ and $\xi_\parallel(q^2)$ are defined by the

TABLE X. The parameters $r_{1,2}$, m_R^2, and $m_{\rm fit}^2$ describing the q^2 dependence of the $B \to K^*$ form factors in the LCSR approach [18] and $T_3(q^2) = \frac{m_B^2 - m_{K^*}^2}{q^2}(\tilde{T}_3(q^2) - T_2(q^2))$. The fit equations to be used are given in the last column.

	r_1	r_2	m_R^2, GeV^2	$m_{\rm fit}^2$, GeV^2	Fit eq.
V	0.923	−0.511	$(5.32)^2$	49.40	(A7)
A_1		0.290		40.38	(A9)
A_2	−0.084	0.342		52.00	(A8)
A_0	1.364	−0.990	$(5.28)^2$	36.78	(A7)
T_1	0.823	−0.491	$(5.32)^2$	46.31	(A7)
T_2		0.333		41.41	(A9)
$\tilde{T}_3$	−0.036	0.368		48.10	(A8)

relations

$$\xi_\perp(q^2) = \frac{m_B}{m_B + m_{K^*}} V(q^2),$$
$$\xi_\parallel(q^2) = \frac{m_B + m_{K^*}}{2E_{K^*}} A_1(q^2) - \frac{m_B}{m_B + m_{K^*}} A_2(q^2). \quad \text{(A17)}$$

We use the definitions Eqs. (A7)–(A9) and (A17), with parameters given in Table X, to determine the q^2 dependence of $\xi_\perp$ and $\xi_\parallel$.

[1] M. Antonelli, D. M. Asner, D. Bauer *et al.*, arXiv:0907.5386v1.
[2] R. Ammar *et al.* (CLEO Collaboration), Phys. Rev. Lett. **71**, 674 (1993).
[3] A. Ali and A. Ya. Parkhomenko, Eur. Phys. J. C **23**, 89 (2002).
[4] S. W. Bosch and G. Buchalla, Nucl. Phys. **B621**, 459 (2002).
[5] D. Atwood, M. Gronau, and A. Soni, Phys. Rev. Lett. **79**, 185 (1997); B. Grinstein, Y. Grossman, Z. Ligeti, and D. Pirjol, Phys. Rev. D **71**, 011504 (2005); D. Atwood, T. Gershon, M. Hazumi, and A. Soni, Phys. Rev. D **71**, 076003 (2005).
[6] Y. Grossman and D. Pirjol, J. High Energy Phys. 06 (2000) 029.
[7] L. M. Sehgal and J. van Leusen, Phys. Lett. B **591**, 235 (2004).
[8] M. Gronau and D. Pirjol, Phys. Rev. D **66**, 054008 (2002); M. Gronau, Y. Grossman, D. Pirjol, and A. Ryd, Phys. Rev. Lett. **88**, 051802 (2002); J. P. Lee, Phys. Rev. D **69**, 014017 (2004).
[9] D. Atwood, T. Gershon, M. Hazumi, and A. Soni, arXiv: hep-ph/0701021v1; V. D. Orlovsky and V. I. Shevchenko, Phys. Rev. D **77**, 093003 (2008).
[10] T. Mannel and S. Recksiegel, Acta Phys. Pol. B **28**, 2489 (1997); G. Hiller and A. Kagan, Phys. Rev. D **65**, 074038 (2002); G. Hiller, M. Knecht, F. Legger, and T. Schietinger, Phys. Lett. B **649**, 152 (2007).
[11] D. Melikhov, N. Nikitin, and S. Simula, Phys. Lett. B **442**, 381 (1998); F. Krüger, L. M. Seghal, N. Sinha, and R. Sinha, Phys. Rev. D **61**, 114028 (2000); **63**, 019901(E) (2001); C. S. Kim, Y. G. Kim, C.-D. Lu, and T. Morozumi, Phys. Rev. D **62**, 034013 (2000).
[12] A. Ali, P. Ball, L. T. Handoko, and G. Hiller, Phys. Rev. D **61**, 074024 (2000); A. Ali, E. Lunghi, C. Greub, and G. Hiller, *ibid.* **66**, 034002 (2002).
[13] F. Krüger and J. Matias, Phys. Rev. D **71**, 094009 (2005).
[14] C. Bobeth, G. Hiller, and G. Piranishvili, J. High Energy Phys. 07 (2008) 106; U. Egede, T. Hurth, J. Matias, M. Ramon, and W. Reece, *ibid.* 11 (2008) 032.
[15] W. Altmannshofer, P. Ball, A. Bharucha, A. J. Buras, D. M. Straub, and M. Wick, J. High Energy Phys. 01 (2009) 019
[16] U. Egede, T. Hurth, J. Matias, M. Ramon, and W. Reece, arXiv:1005.0571v1.
[17] G. Buchalla, A. J. Buras, and M. E. Lautenbacher, Rev. Mod. Phys. **68**, 1125 (1996).
[18] P. Ball and R. Zwicky, Phys. Rev. D **71**, 014029 (2005).
[19] F. De Fazio, T. Feldmann, and T. Hurth, Nucl. Phys. **B733**, 1 (2006); **B800**, 405(E) (2008); J. High Energy Phys. 02 (2008) 031.
[20] B. Aubert *et al.* (*BABAR* Collaboration), Phys. Rev. Lett. **102**, 091803 (2009).
[21] J.-T. Wei *et al.* (Belle Collaboration), Phys. Rev. Lett. **103**, 171801 (2009).
[22] J. Lefrancois and M. H. Schune, Report No. LHCb-PUB-2009-008, 2009.
[23] J. Charles, A. Le Yaouanc, L. Oliver, O. Pene, and J.-C. Raynal, Phys. Rev. D **60**, 014001 (1999).
[24] M. Beneke and Th. Feldmann, Nucl. Phys. **B592**, 3 (2001).
[25] This means the narrow-width approximation for the $\bar{K}^{*0}$ propagator: $(k^2 - m_{K^*}^2 + i m_{K^*}\Gamma_{K^*})^{-1} \approx -i\pi\delta(k^2 - m_{K^*}^2)$.
[26] C. Amsler, M. Doser, M. Antonelli *et al.*, Phys. Lett. B **667**, 1 (2008).
[27] M. N. Achasov, K. I. Beloborodov, A. V. Berdyugin *et al.*, Phys. Rev. D **68**, 052006 (2003).
[28] Heavy Flavor Averaging Group, http://www.slac.stanford.edu/xorg/hfag/rare/.
[29] C. H. Chen, arXiv:hep-ph/0601019v2.
[30] M. Beneke, Th. Feldmann, and D. Seidel, Nucl. Phys. **B612**, 25 (2001).
[31] N. Cabibbo, Phys. Rev. Lett. **10**, 531 (1963); M. Kobayashi and T. Maskawa, Prog. Theor. Phys. **49**, 652 (1973).
[32] N. Gray, D. J. Broadhurst, W. Grafe, and K. Schilcher, Z. Phys. C **48**, 673 (1990).
[33] K. G. Chetyrkin and M. Steinhauser, Phys. Rev. Lett. **83**, 4001 (1999); K. Melnikov and T. van Ritbergen, Phys. Lett. B **482**, 99 (2000).
[34] A. V. Manohar and C. T. Sachrajda, see the review on quark mass in Ref. [26].
[35] K. G. Chetyrkin, Phys. Lett. B **404**, 161 (1997); J. A. M. Vermaseren, S. A. Larin, and T. van Ritbergen, Phys. Lett. B **405**, 327 (1997).